

Nanoscale doping fluctuation resolved by electrostatic force microscopy via the effect of surface band bending

Shu-Cheng Chin,¹ Yuan-Chih Chang,¹ Chia-Seng Chang,^{1,a)} Wei-Yen Woon,^{2,b)} Li-Te Lin,² and Hun-Jan Tao²

¹*Institute of Physics, Academia Sinica, Taipei 115-29, Taiwan*

²*Taiwan Semiconductor Manufacturing Company, Hsinchu 300-77, Taiwan*

(Received 22 September 2008; accepted 26 November 2008; published online 22 December 2008)

A technique for profiling doping fluctuation around source/drain regions on a sub-45-nm device is demonstrated. The mapping is achieved through the amplitude measurement of electrostatic force microscopy (EFM). A discovery was found that the EFM amplitude signal would reverse due to strong band bending at the doped semiconductor surface. We have illustrated this phenomenon to show its sensitive dependence on the local doping density. Combined with a tailored carbon nanotube modified cantilever, the EFM measurement operated near the critical bias voltage can resolve dopant features <10 nm along the effective channel length. © 2008 American Institute of Physics. [DOI: 10.1063/1.3050521]

The current semiconductor manufacturing industry has demonstrated a trend of continual scaling down in the sizes of modern devices. For metal-oxide-semiconductor field-effect transistors (MOSFETs), implantation in the source/drain (S/D) regions with nanometer precision becomes more difficult to control. At such a nanometer scale, variation in effective channel length (L_{eff}) versus line edge/width roughness (LER) can easily lead to local bridging of the device, resulting in extremely low threshold voltages and in turn deteriorating the local mismatch performance.¹ Thus, it posed a serious challenge for both the production and characterization engineers. Scanning probe microscopy—such as scanning capacitance microscopy,^{2,3} scanning spreading resistance microscopy,^{4,5} and scanning tunneling microscopy⁶—has given us detailed analyses of cross-sectional and plane view source/drain extension (SDE) profiles over the past decade. However, problems with the nanoscale implantation induced doping fluctuation, which also causes the nonuniformity of the drive current/threshold voltage, have yet to be addressed. For this purpose, we need a high-resolution plane view tool to map out the surface dopant concentration around S/D regions. In the recent development along this line, carbon nanotube probed electrostatic force microscopy (CNT-probed EFM)^{7–9} proved to be a promising tool in plane view dopant profiling of a modern device.¹⁰

In this paper, we apply a high-quality CNT-modified cantilever into the EFM measurement. The CNT, 350 nm in length and 20 nm in diameter, was attached onto a commercial PtIr/Cr-coated n^+ -Si cantilever inside an ultrahigh vacuum transmission electron microscope (TEM) chamber. Figure 1(a) shows the TEM image of our CNT probe, where the tube apex has been *in situ* trimmed to 5 nm in diameter after its attachment. Our sample, a complementary MOSFET (CMOS) device, is fabricated in SiO₂ gate patterns with n -type (arsenic) implantation at ~ 2 keV with a dose $\sim 10^{15}$ cm⁻² in S/D regions on a striped hard mask patterned

silicon wafer, using the state-of-the-art semiconductor manufacturing process flow. No spacer was formed prior to the implantation so there is intentional lateral diffusion under the gate pattern during the conventional rapid thermal annealing treatment. This doping level near the surface ($\sim 10^{21}$ cm⁻³) is obviously much higher than that for a conventional MOSFET device. Thus, the doping uniformity is harder to achieve and the inhomogeneous implantation in S/D regions becomes more predominant in electronic performance. The apparent gate of our sample measured from the scanning electron microscopy (SEM) image [Fig. 1(b)] is about 45 nm in width and 100 nm in height.¹⁰

In order to map out the local dopant concentration around the SiO₂ gates, we initially etched the SiO₂ gates with a dilute aqua (HF mixed with water at the ratio of 1 to 200) for 40–60 min. The gates were etched away and so were the doped Si in S/D regions due to the isotropic etching of HF.¹⁰ However, our main interest is focused on the area around the undergate region. The entire EFM experiment was done with a commercial atomic force microscopy (AFM)/EFM system, Asylum Research MFP-3D, operating at the lift mode with a user defined lift height of 70 nm.¹⁰ It is also equipped with an adjustable tip bias, a grounded sample holder, and an open feedback loop during EFM scans. The AFM image in Fig. 2(a) shows the topography of one of the three gates in Fig. 1(b) after the isotropic HF etching, where the gate/Si boundaries were etched faster than other flat S/D regions. Such an etched topography is helpful for us to locate the original gate positions. The EFM phase image in Fig. 2(b), with the tip

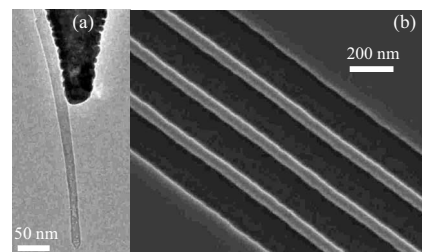


FIG. 1. (a) TEM image of the CNT-modified cantilever employed in this work. (b) SEM image of our sample showing a CMOS structure.

^{a)}Electronic mail: jasonc@phys.sinica.edu.tw.

^{b)}Present address: Department of Physics, National Central University, Zhongli, Taoyuan 320-01, Taiwan.

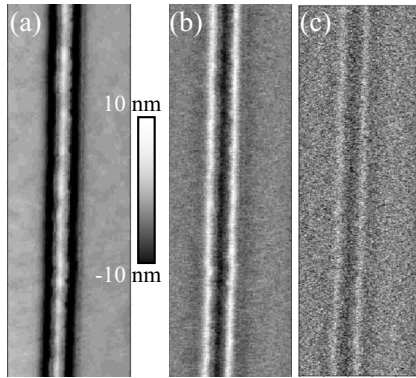


FIG. 2. ($1.5 \times 0.5 \mu\text{m}^2$) (a) AFM topographic image of the sample after HF treatment. (b) EFM phase and (c) amplitude images display the dopant distribution in the undergate area.

biased at 3 V, clearly demonstrates the dopant distribution under the gate, revealing weak SDE and no S/D overlapping in this device. A comparison between the corresponding EFM phase [Fig. 2(b)] and amplitude [Fig. 2(c)] images reveals the fact that the phase image normally provides a better resolution.^{11,12} This is the reason why some EFM-related researchers have chosen only the phase measurement so far. Nevertheless, our major concern in this work is to discern the dopant concentrations along the gate boundaries, where neither Fig. 2(b) nor Fig. 2(c) displays such a contrast.

Intuitively, the EFM amplitude change is a direct response to the electrostatic induction when bias is applied. In contrast, the phase signals are related to the sinusoidal function within the power dissipation spectrum of the tip-sample interaction,¹³ whose relation to the applied electrostatic field is not straightforward.^{12,14,15} Therefore, we employ amplitude measurement while ramping the tip bias up from 0 to 10 V. In Fig. 3(a), the amplitude signals from 5 to 8 V are displayed and a signal inversion between 6 and 7 V is discovered. Unlike the increase in the amplitude signal from 0 to 4 V, the amplitudes acquired at 5 and 6 V seem weaker. The amplitude even switches from the positive response to the negative when the tip bias reaches 7 V. This is clearly demonstrated with Fig. 3(b) where the precise bias for the apparent contrast reversal occurs between 6 and 6.5 V. No such inversion was found when the applied tip bias is in the negative range up to -10 V [Fig. 3(c)].

With the above evidence, this phenomenon can be described by the following scenario. The highly doped areas near the gate edge are normally positively charged due to the donor dopants (here are As^+ ions). These positively charged ions cannot be effectively screened and thus impart a repulsive force to the tip, and the force grows with the bias. Meanwhile this electric field will also have an effect on the nearby regions of these dopants. When the tip bias increases to a point, where the substrate electrons start to flow toward the region under the tip, the reaction of the tip begins to change. In a technical term, this phenomenon is associated with the surface band bending under the influence of electric field introduced by the tip. The flown-in electrons will screen out the field of ions and offset the repulsive force between the tip and dopant ions. The influence will continue and eventually supersede the ion effect. The force felt by the tip turns from the repulsive to attractive and the image contrast reverses. This property about electrostatic force reversal from the repulsive to attractive has been discovered by Park *et al.*¹⁶ for

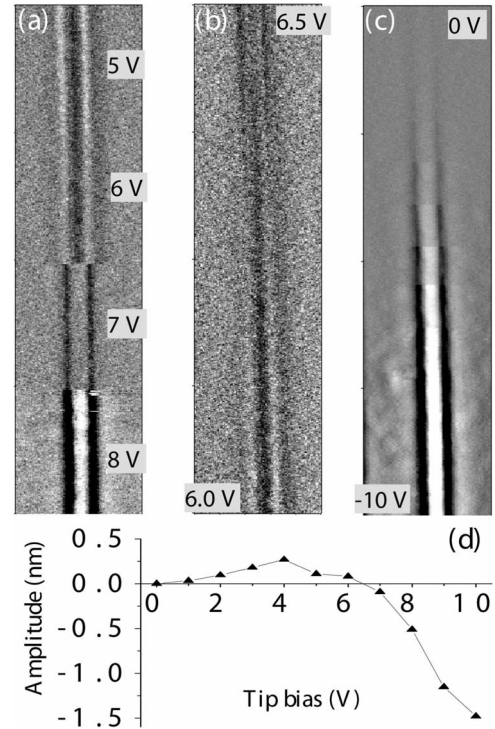


FIG. 3. EFM amplitude images ($2 \times 0.5 \mu\text{m}^2$) (a) taken from 5 to 8 V, (b) taken with the zoom-in bias range of 6.0–6.5 V, and (c) taken in the negative bias range up to -10 V. (d) Plot of the apparent amplitude change as a function of the bias voltage.

the surface dipole across an atomic step. Though some steps may have been resulted at the etched trenches after HF treatment [Fig. 2(a)], the biased tip is lifted 70 nm from the sample in our EFM measurement whereas the tip-sample distance is <1 nm for the electron tunneling experiment of Park *et al.* In detail, the lifted height 70 nm is so chosen to make sure of no force interaction between the unbiased tip and sample, neither van der Waals nor original existing dipole forces. The effect due to cross-step dipoles, if any, should have only generated diffusive contrast along the trenches, and should not fluctuate like what appears in Fig. 4(a). We thus believe that our measured EFM data are predominantly contributed from the dopant behavior near the surface.

In order to maximize the resolution of local dopant concentration under the gate, we choose to lock the bias voltage

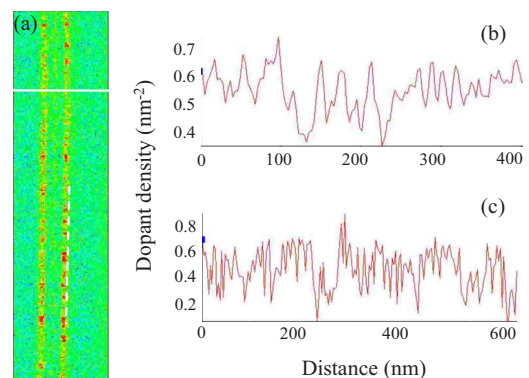


FIG. 4. (Color online) (a) EFM amplitude image ($1.6 \times 0.4 \mu\text{m}^2$) taken near the critical bias, showing clear contrast of dopant concentration along the gate edges. (b) and (c) The line scans taken from the cross white line and the dashed line as indicated in (a), demonstrating a superior contrast.

close to the critical point, where it provides the most sensitive contrast change as shown in Fig. 3(d). The cross point from positive to negative response in Fig. 3(d) can be pinned near 6.4 V. Figure 4(a) recorded the EFM amplitude image at the bias of 6.6 V and distinguishable variations in the dopant concentration along both gate edges are clearly displayed. The line scan plotted in Fig. 4(b), indicated by the white line in Fig. 4(a), confirms that the nanoscale dopant distribution can result in ill-defined L_{eff} , which can further undermine the device performance. Recently, Xiong *et al.*¹ and Fukutome *et al.*⁶ demonstrated through their computer modeling and experimental results that the lateral shape of SDE may fluctuate and may not follow the lateral shape of LER. Here, we have further resolved the variation in dopant concentration along the LER under 10 nm and it is shown in Fig. 4(c). There the amplitude profile of a portion of the right gate edge, indicated by the dashed line in Fig. 4(a), is depicted. This extra information about local S/D dopant concentration should help the frontier device examination besides the L_{eff} data.

We take advantage of the image charge concept to derive some quantitative physical values in reference to the *generalized image charge method*.¹⁶ The force sensed by the charge/tip can be formulated as below

$$F = \frac{1}{4\pi\epsilon_0} \left[\frac{-q^2}{(2D)^2} + \frac{qQ}{D^2} \right] = \frac{1}{4\pi\epsilon_0} \frac{q \left(Q - \frac{q}{4} \right)}{D^2} \propto \frac{Q - \frac{q}{4}}{D^2}, \quad (1)$$

where the tip-sample distance is D , the positive charge accumulating at the biased CNT tip is q with an image negative charge $-q$ at the distance D under the surface, and finally the positive charge coming from the donor ion cores (As^+) at the surface is Q . The tip-sample electric field magnitude comes from the tip bias divided with the tip-sample distance (6.6 V/70 nm). This is under an assumption that the electrical field emitted from CNT apex is very convergent and almost perpendicular to the surface; thus the tip and sample can be regarded as a pair of circular parallel plates with a diameter of 5 nm, corresponding to the *in situ* trimmed CNT apex. The force is obtained with the cantilever parameters, of which the spring constant is 3.4 ± 0.3 N/m by thermal measurement, and the displacement of Fig. 4(a) is 6.0 ± 0.2 nm, in reference to the unbiased EFM amplitude image. From Eq. (1), our calculation shows the charge den-

sity $Q \sim 0.6 \pm 0.3 \text{ nm}^{-2}$, consistent with the dopant density ($\sim 10^{-21} \text{ cm}^{-3}$) near the surface S/D region.

In conclusion, a phenomenon about the signal inversion during the EFM amplitude measurement on a doped semiconductor surface has been utilized to map out the local dopant concentration around the gate edges on a sub-45-nm CMOS device. The inversion point has been traced at the tip bias of 6.4 V. This amplitude measurement is able to achieve advancement in defining the parameters of L_{eff} and local S/D dopant concentrations for the development of modern nanoscale devices. We believe such a CNT-probed EFM technique can be conveniently exploited in the semiconductor industry.

We would like to thank our colleagues Yu-Sheng Ou, Yi-Ru Chang, Chen-Chih Hsu, and Wei-Hsiang Lin in IPAS, and Chih-Ann Yih from UCLA for helpful discussions. This work is supported by the 2007 AS-TSMC joint project.

- ¹S. Xiong and J. Bokor, *IEEE Trans. Electron Devices* **51**, 228 (2004).
- ²K. Kimura, K. Kobayashi, H. Yamada, K. Matsushige, and K. Usuda, *J. Vac. Sci. Technol. B* **24**, 1371 (2006).
- ³C. Y. Nakakura, P. Tangyonyong, D. L. Hetherington, and M. R. Shaneyfelt, *Rev. Sci. Instrum.* **74**, 127 (2003).
- ⁴L. Zhang, K. Ohuchi, K. Adachi, K. Ishimaru, M. Takayanagi, and A. Nishiyama, *Appl. Phys. Lett.* **90**, 192103 (2007).
- ⁵P. Eyben, D. Alvarez, M. Jurczak, R. Rooyackers, A. De Keersgieter, E. Augendre, and W. Vandervorst, *J. Vac. Sci. Technol. B* **22**, 364 (2004).
- ⁶H. Fukutome, Y. Momiyama, T. Kubo, Y. Tagawa, T. Aoyama, and H. Arimoto, *IEEE Trans. Electron Devices* **53**, 2755 (2006).
- ⁷S. D. Tzeng, C. L. Wu, Y. C. You, T. T. Chen, S. Gwo, and H. Tokumoto, *Appl. Phys. Lett.* **81**, 5042 (2002).
- ⁸S. B. Arnason, A. G. Rinzier, Q. Hudspeth, and A. F. Hebard, *Appl. Phys. Lett.* **75**, 2842 (1999).
- ⁹N. R. Wilson and J. V. Macpherson, *J. Appl. Phys.* **96**, 3565 (2004).
- ¹⁰S. C. Chin, Y. C. Chang, C. C. Hsu, W. H. Lin, C. I. Wu, C. S. Chang, T. T. Tsong, W. Y. Woon, L. T. Lin, and H. J. Tao, *Nanotechnology* **19**, 325703 (2008).
- ¹¹M. W. Nelson, P. G. Schroeder, R. Schlaf, and B. A. Parkinson, *J. Vac. Sci. Technol. B* **17**, 1354 (1999).
- ¹²C. H. Lei, A. Das, M. Elliott, and J. E. Macdonald, *Nanotechnology* **15**, 627 (2004).
- ¹³J. P. Cleveland, B. Anczykowski, A. E. Schmid, and V. B. Elings, *Appl. Phys. Lett.* **72**, 2613 (1998).
- ¹⁴E. Strassburg, A. Boag, and Y. Rosenwaks, *Rev. Sci. Instrum.* **76**, 083705 (2005).
- ¹⁵J. Colchero, A. Gil, and A. M. Baró, *Phys. Rev. B* **64**, 245403 (2001).
- ¹⁶J. Y. Park, G. M. Sacha, M. Enachescu, D. F. Ogletree, R. A. Ribeiro, P. C. Canfield, C. J. Jenks, P. A. Thiel, J. J. Sáenz, and M. Salmeron, *Phys. Rev. Lett.* **95**, 136802 (2005).